Available online at www.sciencedirect.com
SCIENCE DIRECT®
Talanta 66 (2005) 92–102
Talanta
www.elsevier.com/locate/talanta

Continuous-flow system for horseradish peroxidase enzyme assay comprising a packed-column, an amperometric detector and a rotating bioreactor

Eloy Salinas[a], Angel A.J. Torriero[a,*], María I. Sanz[a], Fernando Battaglini[b], Julio Raba[a]

[a] *Department of Chemistry, National University of San Luis, Chacabuco 900 y Pedernera, 5700 San Luis, Argentina*
[b] *INQUIMAE–University of Buenos Aires, Ciudad Universitaria, Pabellón 2, 1428 Buenos Aires, Argentina*

Received 10 August 2004; received in revised form 4 October 2004; accepted 6 October 2004
Available online 23 November 2004

Abstract

The roles of chemical kinetics and mass transfer in three types of bioreactors (packed-column reactors, rotating disk bioreactors and amperometric detector), used with continuous-flow sample/reagent(s) processing, are discussed in detail. A normalized quantitative comparison between these types of reactors clearly shows that rotating disk reactors afford a significantly more efficient utilization of active sites and permit the effective utilization of very small amounts of biocatalysts. Horseradish peroxidase (EC 1.11.1.7), in presence of hydrogen peroxide catalyses the oxidation of $[Os(bpy)_2Cl(pyCOOH)]Cl$. The electrochemical reduction back of this cosubstrate is detected on glassy carbon electrode surface at 0.00 V. Furthermore, the critical effect of substrate and cosubstrate concentration on amperometric immunosensors construction in which HRP is used as an enzymatic label was studied.

Keywords: Horseradish peroxidase; Osmium; Flow system; Packed-column reactors; Rotating disk bioreactors

1. Introduction

Horseradish peroxidasa (HRP) (donor: hydrogen peroxide oxireductase, EC 1.11.1.7) is an extracellular plant enzyme involved in the formation of free radical intermediates for the polymerization and cross-linking of cell wall components, for the oxidation of secondary metabolites essential for certain pathogenic defense reactions, and for the regulation of cell growth and differentiation [1]. There are more than 30 isoforms of HRP. Which are usually classified, according to isoelectric point, into three major groups: acidic, neutral, and basic [2]. The slightly basic (cationic) horseradish peroxidase (HRP-C) is the most studied isoform, since it constitutes approximately 50% of the peroxidase content of horseradish root and is commercially available because of its use in clinical analysis and biotransformations [3–5].

HRP-C is a monomeric (M_r of 33,922), glycosylated (18% by mass) enzyme that contains a single high spin ferric protoporphyrin IX prosthetic group and two calcium ions [6–8] that are necessary for competent folding of the recombinant enzyme after expression in *Eschericia coli* [9]. The normal catalytic cycle for HRP is shown in Scheme 1. E_I and E_2 are the oxidized states of the native ferriperoxidase (E), often referred as compounds I and II, respectively. Q is the reducing substrate and P its oxidized counterpart. The catalytic cycle is initiated by a rapid ($k_1 > 10^7\ M^{-1}\ s^{-1}$) $2e^-$ oxidation of the enzyme by hydrogen peroxide (or other organic peroxides) to the ferric porphyrin (Fe III) of HRP to form the oxyferryl π-cation radical heme ($[Fe^{IV} = O]^{\bullet+}$) intermediate E_1 (iron formal oxidation state: +V) and water. In the second step,

* Corresponding author. Tel.: +54 2652 42 5385; fax: +54 2652 43 0224.
E-mail address: torriero@unsl.edu.ar (A.A.J. Torriero).

0039-9140/$ – see front matter © 2004 Elsevier B.V. All rights reserved.
doi:10.1016/j.talanta.2004.10.002

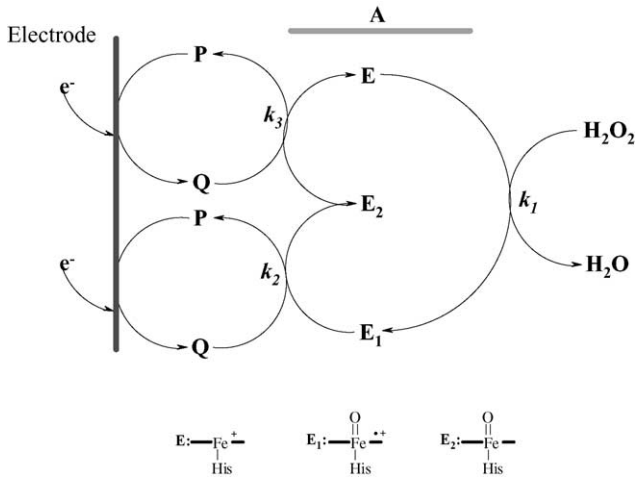

Scheme 1.

the porphyrin radical cation of compound I is reduced by the one-electron donor Q to yield the oxyferryl intermediate E_2 (iron formal oxidation state: +IV) and the product P. In the last step, the enzyme is converted back to its native resting state, E, by a subsequent one-electron/two-proton reduction of E_2 from a second molecule of Q to give a second equivalent of P and water.

Scheme 1 also shows a possible connection of the enzymatic system with an electrode by means of a reversible one-electron mediator couple, P/Q, the reduced form of which, Q, serves as the cosubstrate to the enzyme. The electrochemical response may thus sense the amount of H_2O_2 present in the solution. A good sensitivity is thus expected at potentials where the direct reduction of H_2O_2 is negligible, since the electrochemical response should be enhanced by the catalytic properties of the enzyme. Alternatively, one may use the electrochemical response as a measure of the presence of the enzyme, again taking advantage of the good sensitivity offered by the catalytic properties of the enzyme. Several promising applications based on these principles have indeed been described, and more are likely to appear in the next future. For example, a variety of oxidases (e.g., glucose oxidase, choline oxidase, xanthine oxidase, catechol oxidase, pyruvate oxidase, cholesterol oxidase, etc.), which are able to produce hydrogen peroxide from molecular oxygen during the catalyzed oxidation of their substrates, have been coupled to horseradish peroxidase in several multienzyme amperometric biosensors [10]. HRP-based microelectrodes [11] were also developed for local monitoring of H_2O_2 generated photoelectrochemically [12], electrochemically, or enzymatically [13] at surfaces. The main advantages were the excellent selectivity and sensitivity for H_2O_2 and, once adapted to a scanning electrochemical microscope, the possibility of imaging distributions of catalytic activity on the surface [13].

Most applications that exploit the catalytic current response to reveal the presence of HRP concern amperometric immunosensors in which HRP is used as an enzymatic label [14–17]. In these systems, the specific molecular recognition between an antigen and an antibody assembled on the electrode surface is translated into an electrochemical signal by means of the electrocatalytic activity of the HRP label attached to the immunocomplex.

Transduction of HRP catalysis into an electrochemical signal [18] may involve direct electron transfer from the electrode to the oxidized forms of HRP [19–22]. It may also make use of a mediator that shuttles electrons from the electrode (Scheme 1) to the enzyme, which is either present in the solution [23–25] or immobilized [26–28] (A, Scheme 1).

Previous to the development of the unsegmented flow systems, the preparations of soluble or immobilized enzymes were discussed largely. Investigations carried to the following conclusions: The inexpensive and relatively stable enzymes can be used in convenient form in closed systems and directly in dissolution. Alternatively the miniaturization and the zones confluences use are recommended, in open systems. The relatively expensive or unstable enzymes can be utilized in immobilized form [29]. In other systems, the enzyme is "wired" to the electrode by means of an electron-hopping redox polymer or hydrogel or by other conducting systems [30–32].

The design and performance of reactors utilizing immobilized enzymes as analytical reagents for use with continuous-flow sample/reagent(s) processing attract considerable contemporary interest among analytical chemists. The use of immobilized enzymes in clinical, food, and environmental analyses justifies such interest as well as the publication of specialized monographs [33]. Consequently, in the design of bioreactors for chemical analysis, configurations that afford the maximum utilization of the immobilized active sites are a desirable goal. For both segmented and unsegmented continuous-flow systems, packed-column reactors are by far the most common. These reactors, however, preclude the full utilization of all immobilized active sites. Despite relatively long residence times in the reactor (low flow rates), the geometric configuration of the packing and diffusional constraints do not permit full utilization. In addition, effects of the popularity of packed-column bioreactors stems from the ease of preparation and insertion in continuous-flow manifolds; however, alternatives (e.g., rotating reactors [34]) involve relatively little added complication and, as demonstrated in this article, afford a considerably fuller utilization of immobilized active sites. Mass transport (diffusion/convection) and chemical kinetics are the physicochemical factors that dictate the degree of utilization of active sites, and a discussion of them was included to introduce the comparison between these systems presented here. Furthermore, the critical effect of substrate and cosubstrate concentration on amperometric immunosensors in which HRP is used as an enzymatic label was studied with the intention of proposing adequate criteria to take into consideration in the immunoreactor construction to be applied in a delivered disease's evaluation.

2. Experimental

2.1. Reagents and solutions

All reagents used, except as noted, were of analytical reagent grade. Horseradish peroxidase [EC 1.11.1.7] Grade II was purchased from Sigma Chemical Co., St. Louis. The concentration of HRP was determined spectrophotometrically using the Soret extinction coefficient of 102 mM^{-1} cm^{-1} at 403 nm (10,000 IU = 55 mg). The glutaraldehyde used was purchased from Merk, Darmstadt. 3-Aminopropyl-modified controlled-pore glass, 1400 Å mean pore diameter and 24 m^2 mg^{-1} surface area, was from Electro-Nucleonics (Fairfield, NJ) and contained 48.2 μM g^{-1} of amino groups. $[Os(bpy)_2Cl(pyCOOH)]Cl$ was synthesized as previously described [35]. Aqueous solutions were prepared using purified water from a Milli-Q-system and the samples were diluted to the desired concentrations using a 10 ml Metrohm E 485 burette.

2.2. Apparatus

The main bodies of the bioreactor-amperometric detection unity were made of Plexiglas. Fig. 1 illustrates the design of the flow-through chamber containing the rotating enzyme reactor and the detector system. Glassy carbon electrode is on the top of the rotating reactor. The rotating reactor is a disk of Teflon in which a miniature magnetic stirring bar (Teflon-coated Micro Stir bar from Markson Science Inc., Phoenix, AZ) has been embedded. Rotation of the lower reactor was effected with a laboratory magnetic stirrer (Metrohm E649 from Metrohm AG Herisau, Switzerland) and controlled with a variable transformer with an output between 0 and 250 V and maximum amperage of 7.5 A (Waritrans, Argentina). Fig. 2 illustrates the design of the flow-through chamber containing the amperometric detector system. Glassy carbon electrode is on the top of the detector. Change in cell volume was accomplished by addition of a gasket of several thickness that changed the relative position of the upper cell body with respect to the lower cell body with the unit assembled. The volume of the cell can change from 3.5 to 200 μl. The potential applied to the working electrode was 0.00 V versus Ag/AgCl, 3.0 M NaCl reference electrode, and a Pt wire

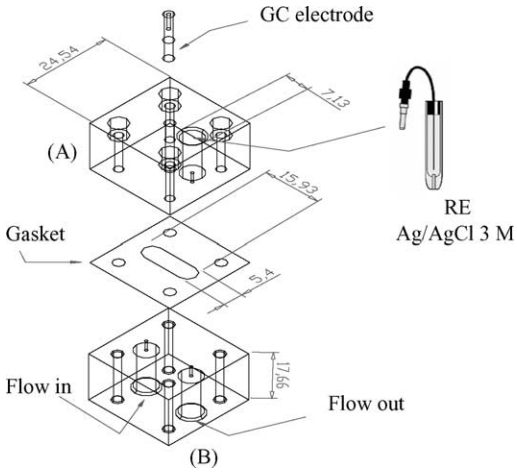

Fig. 2. Schematic representation of components in the amperometric cell. (A) Upper cell body containing the glassy carbon and reference (RE-6) electrodes. (B) Lower cell body. All measurements are given in millimeters.

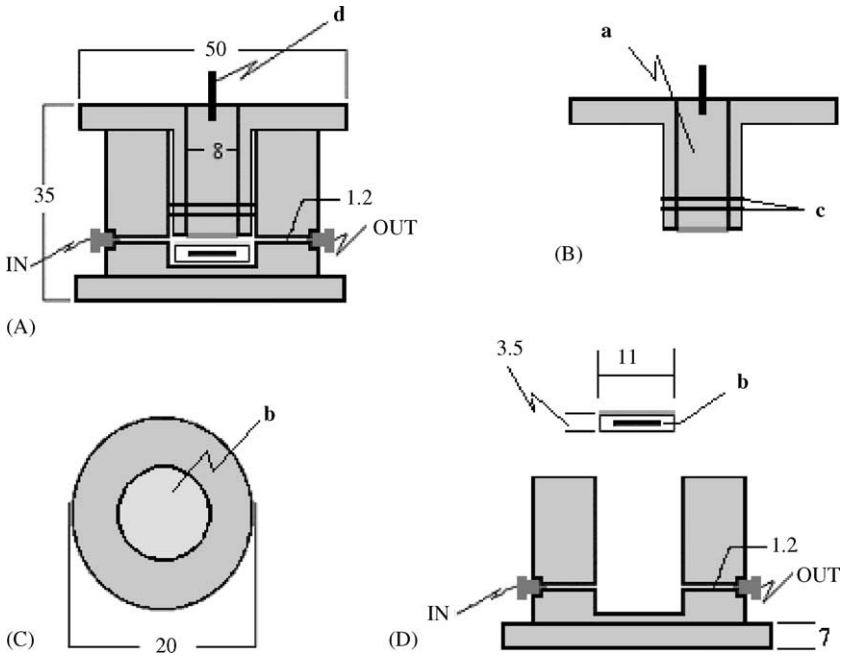

Fig. 1. Schematic representation of components in the bioreactor flow cell. (A) Assembled reactor; (B) upper cell body; (C) top view of lower cell body; (b) rotating bioreactor (with immobilized HRP); (D) lower cell body; (a) glassy carbon electrode; (b) rotating bioreactor; (c) O-ring; (d) electrical connection. All measurements are given in millimeters.

was used as counter electrode. At this potential, a catalytic current was well established. Microcolumns were made of Tygon tubing (2.0 cm long, 2.0 mm i.d.).

A pump (Gilson Minipuls 3 peristaltic pump, Gilson Electronics Inc., Middleton, WI) was used for pumping, sample introduction, and stopping of the flow. Fig. 3 illustrates schematically the components of the single-line continuous-flow setup. The pump tubing was Tygon (Fisher AccuRated, 1.0 mm i.d., Fisher Scientific Co., Pittsburgh, PA) and the remaining tubing used was Teflon, 1.00 mm i.d. from Cole-Parmer (Chicago, IL).

Spectrophotometric measurements, for activity determination, were performed with a Beckman DU 350 UV–vis spectrophotometer and using 1 cm glass cells. All pH measurements were made with an Orion Expandable Ion Analyzer (Orion Research Inc., Cambridge, MA) Model EA 940 equipped with a glass combination electrode (Orion Research Inc., Cambridge, MA).

2.3. Horseradish peroxidase immobilization

HRP was immobilized on 3-aminopropyl-modified controlled-pore glass (APCPG). The APCPG, was allowed to react with an aqueous solution of 5% (w/w) glutaraldehyde at pH 10.00 (0.20 M carbonate) for 2 h at room temperature. After washing with purified water and 0.10 M phosphate buffer of pH 7.00, the enzyme was coupled to the residual aldehyde groups in phosphate buffer (0.10 M, pH 7.00) overnight at 5 °C. The immobilized enzyme preparation was finally washed with phosphate buffer (pH 7.00) and stored in the same buffer at 5 °C between uses. The immobilized HRP preparations were perfectly stable for at least one months of daily use. The same stock preparation was used throughout the overall work comparing packed column and rotating disk.

2.4. Preparation of reactors

Immediately after measurement of the normalized activity, a portion of the enzyme preparation was fixed on the rotating reactor with double-coated sticking tape, and another portion was used as slurry to pack well the column reactor. The weight of immobilized-enzyme preparation contained in each reactor was accurately determined by weighing, with an uncertainty of ±0.05 mg.

3. Results and discussion

3.1. Broad features of the amperometric detection of HRP in the presence of peroxide and osmium complex

We decided to start our study with the case where the enzyme is present in the solution, rather than immobilized, in the aim of disposing of a quantitatively analyzed mechanism, deprived of any of the ambiguities that may arise from the immobilization procedure.

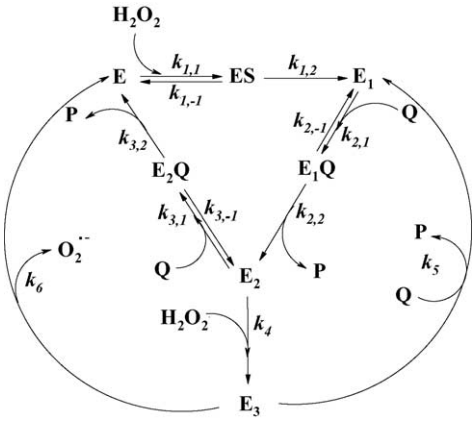

Scheme 2.

Fig. 4 shows a typical set of amperometric peaks currents obtained with increasing concentrations of H_2O_2. These peaks currents were recorded 20 min after the mixing of the reactants so as to ensure that a steady state between the various forms of the enzyme is established before starting the measured at potential constant using the system depicted in Fig. 3. We start in the absence of hydrogen peroxide. Upon addition of H_2O_2, the peak current increases. At higher values of H_2O_2 concentration, the peak current decreases. This decrease in the catalytic current observed upon raising the concentration of H_2O_2 is due to some form of inhibition of the enzyme.

In view of its complexity, it seems necessary to proceed by a step-by-step analysis of the mechanism. In the primary catalytic cycle of HRP (Scheme 2), the kinetics of the reaction of E with H_2O_2 to yield E_1 has been investigated extensively [36,37]. Although evidence has been previously gathered that the kinetics follows a Michaelis–Menten behavior [38], it is only recently that its characteristics have been unambiguously determined [39], leading to $K_{1,M} = (k_{1,-1} + k_{1,2})/k_{1,1})$ 128 μM and to a confirmation of the k_1 value, i.e., $k_1 = k_{1,1}k_{1,2}/(k_{1,-1} + k_{1,2}) = 1.7 \times 10^7\ M^{-1}\ s^{-1}$. The reduction of E_1 and E_2 by several electron donors has been reported, although they are in most cases both electron and proton donors, unlike the osmium cosubstrate investigated in the present study. Scheme 2 indicates the possibility of a Michaelis–Menten behavior also for the reduction of E_1 and E_2 in view of the fact that such behavior has been reported for several other cosubstrates [39,40].

Concerning the Michaelis–Menten behavior observed for the E_2/E reaction, it should be emphasized that the reduction of E_2 is not a mere outersphere electron-transfer reaction but rather involves the exchange of one electron and two protons and the cleavage of the iron-oxygen bond (Scheme 3). These reactions, or maybe other mechanistic peculiarities to be uncovered, might be the cause of the observed kinetics showing saturation behavior upon increasing the reactant concentration, which therefore does not necessarily reflect a true Michaelis–Menten mechanism such as the one depicted in Scheme 2.

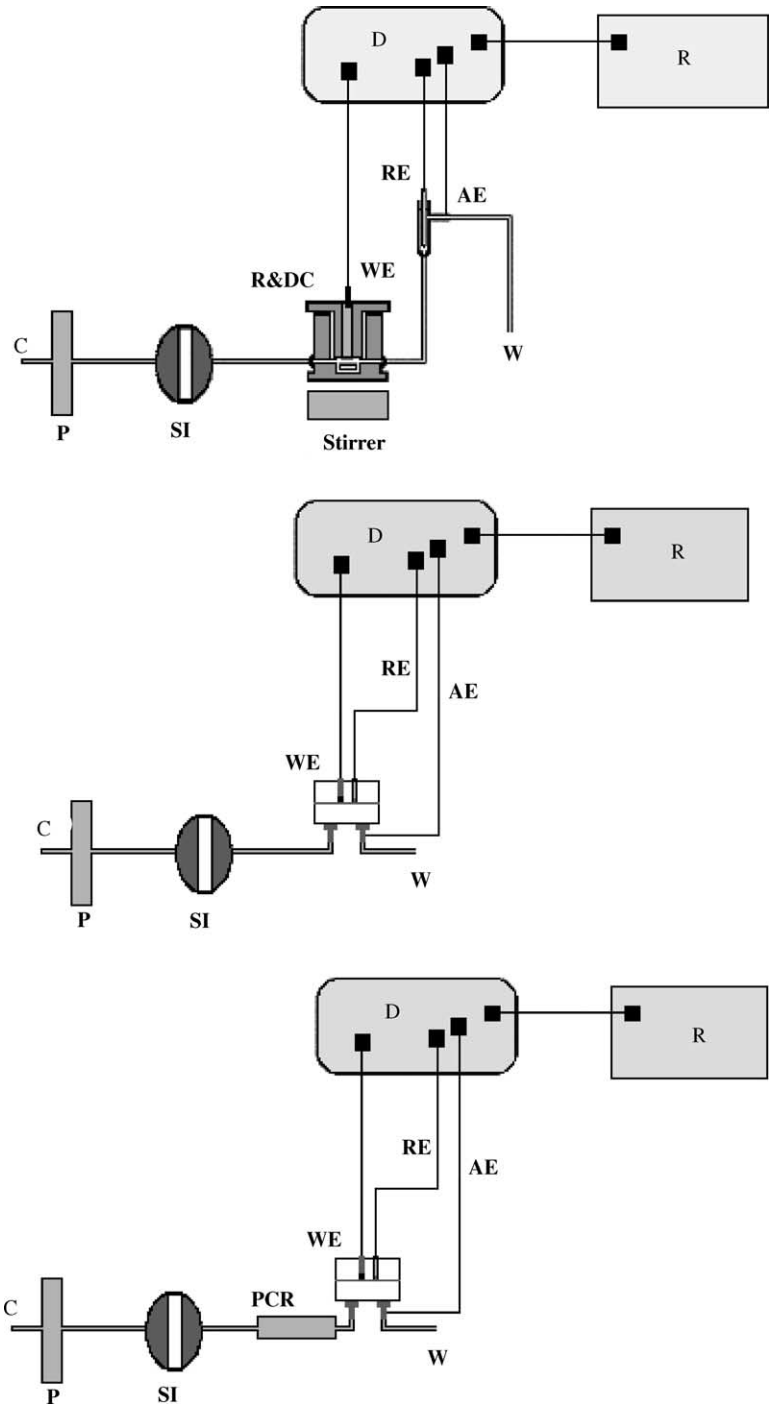

Fig. 3. Block diagrams of the single line continuous-flow systems showing the location of the reactors compared in this work. P: Pump (Gilson Minipuls 3 peristaltic pump, Gilson Electronics Inc., Middleton, WI). C: Carrier buffer line. SI: Sample injection. W: Waste line. R&DC: Reactor and detector cell. WE: working electrode. RE: Reference electrode (Ag/AgCl, 3.0 M NaCl). AE: Auxiliary electrode (stainless steel tubing). D: Potentiostat/detection unit (LC-4C, Bioanalytical Systems, West Lafayette, IN). R: Recorder (Varian, Model 9176, Varian Techtron, Springuale, Australia). PCR: Packed-column reactor.

Inhibition by conversion of the initial enzyme by H_2O_2 into inactive oxyperoxidase, E_3, may occur even in the presence of the oxidized form of the cosubstrate. H_2O_2 may indeed reduce E_1 into E_2, albeit slowly [36], thus opening a route to the conversion of E_2 into E_3. This is the reason for the slow decay of the catalytic current observed in Fig. 4. Two pathways for this inactivation have been previously identified. One is an irreversible set of reactions finally yielding a verdohemoprotein (also designated as P670) [41]. This irreversible inactivation pathway of HRP is insignificant under our experimental conditions. The second pathway involves the formation of oxyperoxidase [42], usually designated as

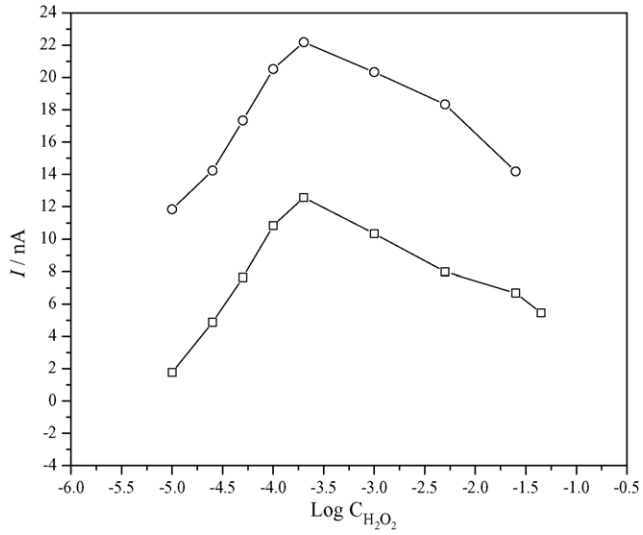

Fig. 4. Variation of the peak current with the concentration of H_2O_2, recorded in phosphate buffer solution (pH 7.0), containing 20 μM [Os(bpy)$_2$Cl(pyCOOH)]Cl, 0.182 mIU ml^{-1} HRP. (□) Peak current with amperometric detector obtained 20 min after the mixing of the reactants. (○) Peak current measured with rotating bioreactor under stopped-flow conditions, reactor rotation velocity, 1600 rpm.

compound III or E_3. This compound, which does not normally participate in the peroxidase activity of HRP, has a structure similar to that of oxyhemoglobin [43] (Scheme 4). In the presence of H_2O_2, the formation of E_3 from the reaction of H_2O_2 with E_2 occurs with a rate constant k_4 ranging from 16 to 40 M^{-1} s^{-1}, depending on pH and temperature [44]. E_3 is not necessarily a dead end to the catalytic cycle of HRP. It is indeed converted back to E by spontaneous decomposition, yielding superoxide ion.

This fact can be observed easily in experimental form varying H_2O_2 concentration from 2.5×10^{-5} to 5.0×10^{-3} M, for 20 μM Q solutions and several concentrations of HRP (Fig. 5). Low H_2O_2 concentration, 0.025 mM, a lineal relation can see only when the enzymes concentrations are low, losing this linearity as increases the enzymatic concentration. That is observed because this H_2O_2 concentration is insufficient to generate maximum catalytic activity. To 0.1 mM H_2O_2 concentration, a perfect linearity in all concentrations range studied is obtained. To 0.5 mM H_2O_2 concentration, linearity is lost to low concentrations. That is because the HRP is inactivated in excess of H_2O_2. At higher H_2O_2 concentration, 5 mM, inhibition by conversion of the initial enzyme by H_2O_2 into E_3 is observed in all HRP concentration range studied. In this case linearity is observed but the catalytic current obtained is less significant than in the optimal case.

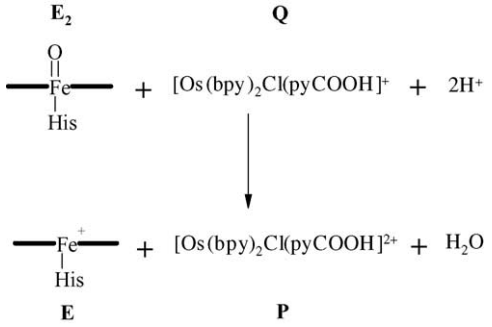

Scheme 3.

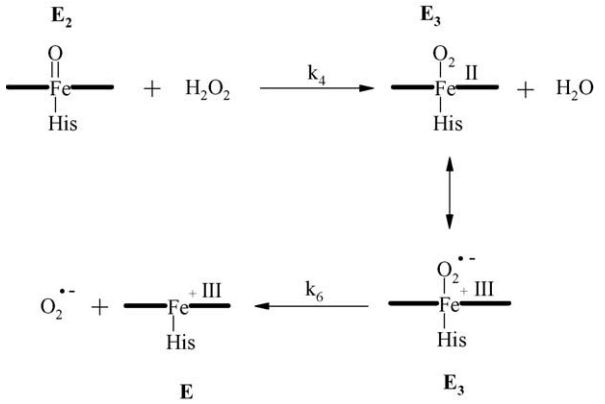

Scheme 4.

The effect of varying osmium complex concentration from 5 to 70 μM, for 0.1 mM H_2O_2 and 1.129 mIU ml^{-1} HRP, were evaluated (Fig. 6). A significant increase can be observed from 5 to 17 μM osmium complex. For greater concentrations insignificant differences were obtained, hence, to avoid analytical uncertainty due to changes in osmium complex concentrations, 20 μM of [Os(bpy)$_2$Cl(pyCOOH)]Cl was used.

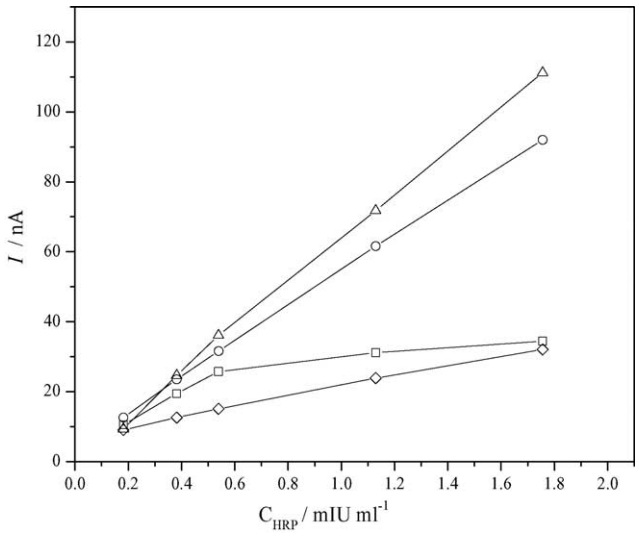

Fig. 5. Catalytic current as a function of the HRP concentration recorded at 0.00 mV vs. Ag/AgCl 3 M in a phosphate buffer (pH 7.00) containing 20 μM [Os(bpy)$_2$Cl(pyCOOH)]Cl, and 0.025 (□), 0.1 (○), 0.5 (△), and 5 (◊) mM H_2O_2.

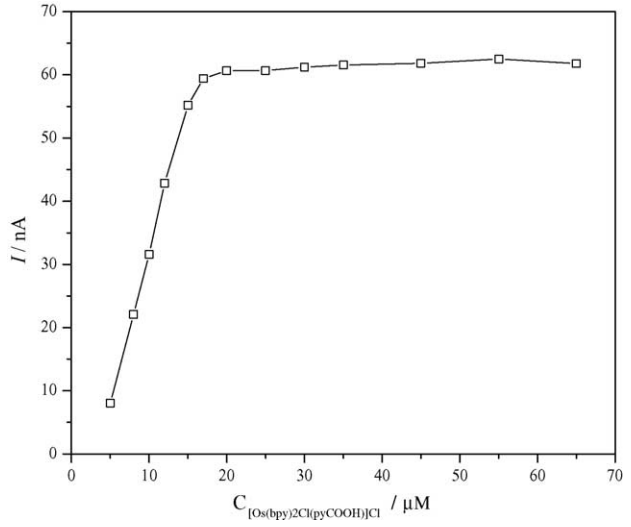

Fig. 6. Effect of osmium complex concentration on the catalytic current: 0.1 mM H_2O_2, 1.129 mIU ml^{-1} HRP, 0.10 M phosphate buffer (pH 7.00).

3.2. Mass transfer using immobilized catalytic centers

Arrival of substrate molecules to the active site of the immobilized biocatalyst is dictated by molecular diffusion within the diffusion (stagnant) layer, ∂, and this is a function of the mass transfer coefficient, $m = D/\partial$ (D is the molecular diffusion coefficient), and the concentration gradient:

$$\frac{d[S_s]}{dt} = m([S_b] - [S_s]) \quad (1)$$

where S_s is the substrate at the surface of the immobilized enzyme preparation (vicinity of enzyme active site) and S_b is the substrate in the bulk of the solution. A decrease in the thickness of the diffusion layer, ∂, and an increase in concentration gradient, $[S_b] - [S_s]$, will result in an increase in the rate of substrate arrival at the site where the immobilized enzyme resides.

Experimental conditions in unsegmented continuous-flow systems result in predominantly laminar flow within the sample plug containing the analyte [45]. In laminar flow, each layer of solution flows in parallel paths; solutes diffuse through each layer and the diffusion layer to reach the active site, while in turbulent flow solutes diffuse directly from the bulk solution through the diffusion layer. As such, the concentration gradient developed within the diffusion layer boundaries is larger under turbulent than laminar flow conditions. Turbulent flow, however, would remove the advantages of reasonable residence times within the packed column afforded by laminar flow. It would also increase back-pressure problems if a small-particle-size packing material is used to increase the nominal activity of the immobilized enzyme and compensate for a short residence time. In other words, turbulent flow complicates matters under continuous-flow operation [46].

Since the inert supports used to anchor the biocatalyst are not ideally smooth, formation of local turbulence is realized at any irregularities or pronounced curvatures. Local turbulence at cylindrical/spherical bodies, protruding surface irregularities, sharp bends, or surface depressions in packed columns develop at Reynolds numbers, *Re*, between 1 and 100 [47]. Hamilton et al. [48] have quoted *Re* values in the range 0.003–0.2 (velocity up to 0.18 cm s^{-1}), and values of $Re \approx 20$ are needed for turbulence around protruding surface irregularities [49]. Average velocities in typical flow injection systems are three to four times as high; hence, one would suspect that, when using packed columns of 1–2 mm i.d. and flow rates of about 1.0 ml min^{-1}, local *Re* numbers should be barely below 1 or 1 at most. Therefore, local turbulence would rarely be encountered with packed columns and unsegmented continuous-flow processing. Local turbulence, if present, would not help in improving the diffusional constraints of mass transfer when using the typical packed-column reactors, and strategies incorporating convectional mass transfer should provide a competitive alternative. The discussion presented here is on substrate and cosubstrate arrival at the active site; similar considerations are also applied to transport of the product of the enzyme-catalyzed reaction from active site to the bulk of the solution.

3.3. Kinetics for immobilized catalytic centers

Eq. (1) mathematically describes the arrival of substrate at the active site. The conversion of substrate to products, with the participation of the enzyme active site, is equally important. The apparent Michaelis–Menten constant is represented by K'_M. The fact that imposing rotation to a platform bearing the immobilized enzyme preparation on its surface, and one which is in contact with solution containing the substrate reduces the value of K'_M is well documented [50,51]. Under mass transfer control of the overall process, we can expect that $K'_M \gg [S_s]$, and the rate of conversion to product will be given by:

$$\frac{-d[S_s]}{dt} = \frac{k_{cat}[ES_s][S_s]}{K'_M} \quad (2)$$

As rotation decreases the value of K'_M, the catalytic efficiency, k_{cat}/K'_M, increases, and analytical signals should increase correspondingly. At sufficiently high rotation speeds, it can be expected that $[S_s] \gg K'_M$, and chemical kinetics controls the overall process because $-d[S_s]/dt \approx k_{cat}[ES_s]$. In such a case, the analytical signal should, for all practical purposes, remain constant with increasing rotation velocity. Table 1 illustrates that, indeed, the expected behavior is observed when the rotation velocity of the bioreactor is increased. Table 1 illustrates the trend for a cell volume of 300 μl. The trend indicates that, up to velocities of about 1500 rpm, a decrease in the thickness of the stagnant layer improves mass transfer to and from the immobilized enzyme active sites. Beyond 1500 rpm, the current is constant, and chemical kinetics controls the overall process. It is of interest to note that, although the mass transfer is being realized un-

Table 1
Effect of reactor rotation velocity and cell volume on current measured under stopped-flow conditions

Rotation velocity[a] (rpm)	Current (nA)	Linear regression, standard deviation	Cell volume[b] (μl)	Current (nA)	Linear regression, standard deviation
200	14.238	±0.0453	300	20.518	±0.0010
400	14.920	±0.0757	400	19.666	±0.0020
600	15.867	±0.0860	500	18.810	±0.0040
800	16.935	±0.0310	600	18.244	±0.0010
1000	17.932	±0.0565	700	17.477	±0.0046
1200	19.027	±0.0406	800	16.657	±0.0020
1400	20.014	±0.0818	900	16.013	±0.0025
1600	20.522	±0.0801	1000	14.881	±0.0025
1800	20.518	±0.0500			
2000	20.523	±0.0402			

HRP concentration, 0.182 mIU ml^{-1}, 20 μM osmium complex, 0.10 mM H_2O_2, 0.10 M phosphate buffer of pH 7.00. The flow was stopped for 60 s during measurement.
[a] Cell volume was 300 μl.
[b] Reactor rotation velocity was 1600 rpm.

der conditions similar to a thin-layer bounded diffusion with imposed turbulence, the dependence seems to agree better with the response at a rotating disk electrode and the Levich's equation [52]. Levich's equation, however, is derived for conditions of semi-infinite diffusion (the walls of the "cell" can be considered to be at infinity), and fast laminar flow predominates at the rotating surface.

3.4. Effect of cell volume and sample size

Depending on the volume of the cell in contact with the reactor, the overall process becomes controlled by diffusion (large volumes) or by the chemical kinetics of the enzyme-catalyzed reactions (small volumes). The cell volume was changed from 300 μl to 1 ml by removing the O-rings between the upper and lower half of the cell. In an attempt to minimize the dilution effect, the sample size was changed accordingly to ensure that the entire volume of the cell was filled with the sample. The response, as expected, decreased linearly with an increase in cell volume, due to the dilution effect favoured by rotation, and the fact that the measured current is directly proportional to bulk concentration. The smallest cell volume of 300 μl was adopted for further studies (Table 1).

Same study was performed with the amperometric detector, but in this case the cell volume was changed by increasing the thickness gasket between the working electrode and the lower cell body from 3.5 to 200 μl, with a flow rate of 1.0 ml min^{-1}. The response, as expected, decreased linearly with an increase in cell volume (Table 2). These current obtained was recorded 20 min after the mixing of the reactants so as to ensure that a steady state between the various forms of the enzyme is established before starting the measured at potential constant. Under these conditions, although a chemical equilibrium as been attained, physical process is in evolution when measures are performed. Thus, both the physical processes as the chemicals can provide kinetic character to a process and as a consequence to the analytical method based in it. The smallest cell volume of 3.5 μl was used.

4. Quantitative comparison of catalytic efficiency between rotating bioreactors and conventional packed-column reactors

The comparison was guided by utilizing normalized data and a single batch of enzyme preparation in all the work. These values can be considered to be proportional to the number of enzyme active sites per unit weight of immobilized enzyme preparation in each of the two types of reactors compared. After each measurement of activity, the rotating disk reactor and packed column to be compared were prepared as described in Section 2, and the respective amounts of CPG-E in each type of reactor were ascertained. The reactors were then incorporated into a single line continuous-flow manifold, like those illustrated in Fig. 3. When using the packed-column reactor, the flow rate used was between 1.0 and 1.5 ml min^{-1}, values that are representative of the flow rates used in typical applications of packed reactor in flow injection analyses. Sample transport from injection to detection when using the rotating reactor was at a flow rate of 1.0 ml min^{-1}. The rotation velocity of the disk containing the enzyme preparation

Table 2
Effect of cell volume on amperometric current measured using the amperometric detector

Cell volume (μl)	Current (nA)	Linear regression, standard deviation
3.5	10.830	±0.0015
7	10.543	±0.0012
14	10.398	±0.0015
23	10.092	±0.0025
40	9.204	±0.0030
64	8.618	±0.0015
92	7.634	±0.0020
120	7.374	±0.0015
148	6.103	±0.0026
176	5.395	±0.0049
204	4.449	±0.0020

Flow rate 1.0 ml min^{-1}, HRP concentration, 0.182 mIU ml^{-1}, 20 μM osmium complex, 0.10 mM H_2O_2, 0.10 M phosphate buffer of pH 7.00. The current was recorded 20 min after the mixing of the reactants.

Table 3
Comparative (normalized) enzymatic efficiency of rotating and packed-column bioreactors[a]

Normalized activity (mIU)	Normalized signal, nA (mIU)$^{-1}$		
	Rotating reactor	Packed-column reactor	
		Flow rate 1.0 ml min^{-1}	Flow rate 1.5 ml min^{-1}
1.129 ± 0.01	81.755 ± 0.02	6.289 ± 0.02	4.864 ± 0.01
1.129 ± 0.02	81.648 ± 0.02	5.832 ± 0.01	4.575 ± 0.02
1.129 ± 0.01	81.759 ± 0.05	6.056 ± 0.02	4.759 ± 0.01
1.130 ± 0.02	81.669 ± 0.05	5.897 ± 0.03	4.675 ± 0.01
1.130 ± 0.02	81.701 ± 0.03	6.144 ± 0.02	4.778 ± 0.02
Mean	81.706 ± 0.05	6.044 ± 0.02	4.730 ± 0.01

[a] Uncertainties given as sample standard deviations of at least eight independent measurements.

was 1600 ± 20 rpm. The injection volume in both cases was 300 μl, which completely filled the electrochemical cell used for detection. After the electrochemical traces were recorded, the peak intensity was obtained and normalized per unit activity in the corresponding reactor. The units of the normalized response are nanoampere per unit activity [nA (mIU)$^{-1}$]. It must always be remembered that is crucial to all amperometric determinations the Faraday's law, which states that:

$$Q = nFN \tag{3}$$

where Q is the number of Coulombs (a unit of charge) used in converting N moles of material, n is the number of moles of electrons lost or gained in the transfer process per mole of material, and F is Faraday's constant. Differentiation of (3) with respect to time yields the current, which is the measure of the rate at which material is converted:

$$\frac{dQ}{dt} = i = \frac{nF\,dN}{dt} \tag{4}$$

Eq. (4) therefore relates a measurable quantity, the current, to the fundamental redox process occurring in the cell.

The results of five comparative runs are summarized in Table 3. As can be seen from this table, the rotating bioreactor strategy increases by 15–20 times the enzymatic efficiency per active site. Sampling frequency has been and is an analytical figure of merit cited frequently as being significant when continuous-flow sample/reagent(s) processing is utilized. In using the packed-column reactor, the flow rate plays a critical role in dictating the sampling frequency. The time the flow is stopped and the flow rate play the same role when the rotating bioreactor is used. This is because of the signal integration approach used here and the fact that the return to baseline is flow dependent. Consequently, a perfectly normalized comparison is elusive, but some critical comparison is possible. Results for such comparison are summarized in Table 4. Inspection of these tables indicates that a 5 s stopped-flow measurement with the rotating reactor provides sampling rate and enzymatic efficiency comparable to those of the packed column. In actuality, sampling rates close to those observed with the column can be obtained with up to 15 s stopped flow with a double of the biocatalytic efficiency. There is a trade-off, of course, for the rotating reactor between sampling rate and catalytic efficiency. Some sacrifice in the sampling rate must be accepted in order to take advantage of the efficient utilization of the fewer active sites immobilized on the surface of the rotating reactor.

As we have pointed out previously, sampling frequency has been and is significant when continuous-flow sample/reagent(s) processing is used. By using the detector, although 20 min allow significant catalytic current in comparison with rotatory disk (Fig. 4), but this time is unproductive regarding the sampling frequency. Therefore, response of amperometric detector at several times was evaluated (Table 5). An inspection of times indicates that a 5 or 15 s after the mixing of the reactants provides an enzymatic efficiency that can not be comparable to those of the packed column and rotating bioreactor. We conclude that the detector is suitable for enzymatic mechanism analysis, but is not a system comparable

Table 4
Sampling rate and normalized responses with rotating bioreactors as a function of flow rate and time the flow is stopped for acquisition of data[a]

Stopped flow (s)	Flow rate 1.0 ml min^{-1}		Flow rate 1.5 ml min^{-1}	
	Sampling rate (samples h^{-1})	Normalized signal nA (mIU)$^{-1}$	Sampling rate (samples h^{-1})	Normalized signal nA (mIU)$^{-1}$
0	66.2 ± 1.2	3.568	84.9 ± 1.3	2.379
5	54.7 ± 1.1	6.343	63.4 ± 1.3	3.964
10	46.2 ± 1.0	9.911	51.8 ± 1.2	7.929
15	41.9 ± 1.0	15.065	43.2 ± 1.1	12.290
30	30.2 ± 0.8	30.289	33.9 ± 1.2	29.932
60	21.5 ± 0.5	81.669	24.5 ± 0.9	76.515
120	13.5 ± 0.5	216.060	15.1 ± 0.7	185.931
180	10.5 ± 0.4	350.060	11.8 ± 0.6	285.836

[a] Uncertainties given as sample standard deviations of at least five different (but similar) reactors.

Table 5
Response of amperometric detector at several mixing times of the reactants before starting the measured at potential constant

Time (s)	Normalized signal nA (mIU)$^{-1}$	Linear regression, standard deviation
5	1.81	±0.02
15	1.95	±0.02
30	2.42	±0.02
60	3.60	±0.05
120	5.73	±0.06
180	8.87	±0.07
360	17.84	±0.07
600	31.12	±0.08
900	49.07	±0.10
1200	54.57	±0.11

Flow rate 1.0 ml min^{-1}, HRP concentration, 1.129 mIU ml^{-1}, 20 μM osmium complex, 0.10 mM H_2O_2, 0.10 M phosphate buffer of pH 7.00.

to the other two systems, at least using the volumes studied in this work.

5. Comparison of Michaelis–Menten constants and maximum amperometric response in packed-column and rotating bioreactors

As it is reported in previous articles [34], rotation is expected to decrease the value of the apparent Michaelis–Menten constant, K'_M, with a concomitants increase in reaction rates. This makes possible sensitive determinations with relatively very small amount of catalyst. To verify this, the K'_M were evaluated for both types of reactors by using an adaptation of the Lineweaver–Burk plot [34]. Eight individually prepared rotating reactors and eight packed columns were included in this part of the study. As was expected, K'_M values in packed reactors decreased when the length of the column was increased (representing a larger packing of immobilized active sites). The trend in decreasing values of K'_M in packed reactors levels off at about a value of 1.321 mM for packing 14 mg of CPG-E or more (Table 6). A similar trend has been observed during a study of the determination of K_M constants using a variable flow rate approach [53]. Table 6 also shows, as a corollary of the studies reported here, that with a fixed amount of CPG-E, the same can be accomplished by increasing the rotation velocity of the rotating disk bearing the CPG-E.

6. Conclusions

The variation of the electrochemical response with the substrate concentration is, at first sight, perplexing. While for very small concentrations of H_2O_2, the response increases, as expected, with H_2O_2 concentration, a maximum and a descending variation are rapidly observed. This behavior is caused by the reaction of the E_2 form of the enzyme with H_2O_2, forming oxyperoxidase (E_3), which inhibits catalysis. In the framework of the mechanism represented in Scheme 2 and Figs. 4 and 5, conditions such as low H_2O_2 concentrations, can be defined which render inhibition insignificant, but sufficiently high H_2O_2 concentrations are necessary due to very low concentration is unable to generate a maximum catalytic activity. This fact is very important in immunoreactors constructions; because when low antibodies concentrations in the serum sample are allowed to react immunologically with the antigens immobilized on a rotating disk and the bound antibodies are quantified by a HRP enzyme labeled second antibody specific to human IgG, using an osmium complex [Os(bpy)$_2$Cl(pyCOOH)]Cl as enzymatic mediators, the substrate concentrations play a very important role in the adequate calibrations graph constructions.

Another important fact is the similitude in the enzyme's behavior independently if it is in solution or immobilizing on APCPG (Fig. 4). That is not demonstrated in previous works and is of relevant importance in order to do mechanistic study not only with the enzyme in solution.

The relative merits of FIA-amperometric detector are useful if we think in inexpensive enzyme and miniaturized systems. Thus, if we carried the volume of the cell to values lower than 3.5 μl, will be possible find currents of the same order than rotating bioreactors. The only disadvantage that presents this system is the large stabilization time necessary to obtain those currents.

The relative merits of rotating bioreactors in comparison to conventional column-packed reactors for use in conjunction with unsegmented flow sample/reagent(s) processing (e.g., minimal dispersion and maximal utilization of a very small number of immobilized active sites) are clear and are demonstrated in a quantitative manner in the work reported here. These relative merits result from minimization of the limitations imposed by the rate of the enzyme-catalyzed reaction and the interplay of mass transfer in the form of diffusion

Table 6
Values of K'_M (apparent Michaelis–Menten constant)

Rotation velocity (rpm)	K'_M (mM)[a]	Linear regression, standard deviation	Weight of CPG-E (mg)	K'_M (mM)[a]	Linear regression, standard deviation
170	22.030	±0.42	2.0	3.080	±0.14
240	15.310	±0.30	4.5	2.433	±0.09
420	8.675	±0.70	9.0	1.686	±0.10
840	2.871	±0.10	14.0	1.321	±0.25
900	2.270	±0.68	17.0	1.176	±0.18
1000	2.030	±0.42	20.0	1.080	±0.12

Effect of increasing the length of the packed-column reactor (increasing the amount of CPG-E packed) and effect of disk bioreactor rotation velocity.
[a] Each value of K'_M based on eight individually prepared rotating reactors and packed columns.

and forced convection. This interplay and these limitations are introduced in this paper as background for a better understanding of the comparative results presented here.

The rotating reactor showed significant catalytic efficiency.

The rotating reactor showed the better catalytic efficiency, using HRP as enzymatic system. This result agrees with the results found for Richter et al. [46] using glucose oxidase as enzymatic system (in that work, only column-packed reactors was used as comparison system). Therefore, we conclude that the rotating reactor has superior characteristics to the other ones presented in this work, independently of the enzymatic system used.

Acknowledgements

The authors wish to thank the financial support from the Universidad Nacional de San Luis and the Consejo Nacional de Investigaciones Científicas y Técnicas (CONICET). One of the authors (A.A.J.T.) acknowledges support in the form of a fellowship from the Consejo Nacional de Investigaciones Científicas y Técnicas (CONICET), and (F.B.), acknowledges financial support from Fundación Antorchas.

References

[1] C. Penel, T.H. Gaspar, H. Greppin (Eds.), Plant Peroxidases, University of Genova, Genova, Switzerland, 1992.
[2] L.M. Shannon, E. Kay, J.Y. Lew, J. Biol. Chem. 241 (1966) 2166.
[3] H.B. Dunford, J.S. Stillman, Coord. Chem. Rev. 19 (1976) 187.
[4] I. Yamazaki, M. Tamura, R. Nakajima, Mol. Cell. Biochem. 40 (1981) 143.
[5] J. Everse, K.E. Everse, M.B. Grisham, in: H.B. Dunford (Ed.), Peroxidases in Chemistry and Biology, vol. II, CRC Press, Boca Raton, FL, 1991, pp. 1–24.
[6] M.J.R. Marañon, R.B. Van Huystee, Phytochemistry 37 (1994) 1217.
[7] Y. Shiro, M. Kurono, I. Morishima, J. Biol. Chem. 261 (1986) 9382.
[8] I. Morishima, M. Kurono, Y. Shiro, J. Biol. Chem. 261 (1986) 9391.
[9] A.T. Smith, N. Santama, S. Dacey, M. Edwards, R.C. Bray, R.N.F. Thorneley, J.F. Burke, J. Biol. Chem. 265 (1990) 13335.
[10] A.A.J. Torriero, I.E. De Vito, J. Raba, in: H. Fernandez, M.A. Zón (Eds.), Recent Development and Applications of Electroanalytical Chemistry, Research Signpost, Kerala, India, 2002 (Chapter 4).
[11] P. Pantano, T.H. Morton, W.G. Kuhr, J. Am. Chem. Soc. 113 (1991) 1832.
[12] H. Sakai, R. Baba, K. Hashimoto, A. Fujishima, A. Heller, J. Phys. Chem. 99 (1995) 11896.
[13] B.J. Horrocks, D. Schmidtke, A. Heller, A.J. Bard, Anal. Chem. 65 (1993) 3605.
[14] B. Deasy, E. Dempsey, M.R. Smyth, D. Egan, D. Bogan, R. O'Kennedy, Anal. Chim. Acta 294 (1994) 291.
[15] D.J. Pritchard, H. Morgan, J.M. Cooper, Anal. Chim. Acta 310 (1995) 251.
[16] C.J. McNeil, D. Athey, W.O. Ho, Biosens. Bioelectron. 10 (1995) 75.
[17] C.N. Campbell, T. Lumley-Woodyear, A. Heller, Fresenius J. Anal. Chem. 364 (1999) 165.
[18] T. Ruzgas, E. Csöregi, J. Emnéus, L. Gorton, G. Marko-Varga, Anal. Chim. Acta 330 (1996) 123.
[19] R.M. Paddock, E.F. Bowden, J. Electroanal. Chem. 260 (1989) 487.
[20] D.L. Scott, E.F. Bowden, Anal. Chem. 66 (1994) 1217.
[21] W.O. Ho, D. Athey, C.J. McNeil, H.J. Hager, G.P. Evans, W.H. Mullen, J. Electroanal. Chem. 351 (1993) 185.
[22] U. Wollenberger, J. Wang, M. Ozsoz, E. Gonzales-Romero, Bioelectrochem. Bioenerg. 26 (1991) 287.
[23] M.H. Smit, A.E.G. Cass, Anal. Chem. 62 (1990) 2429.
[24] J.M. Cooper, J.V. Bannister, C.J. McNeil, J. Electroanal. Chem. 312 (1991) 155.
[25] Y. Nakabayashi, A. Omayu, S. Morii, S. Yagi, Sens. Actuators B 66 (2000) 128.
[26] S.R. Razola, E. Aktas, J.-C. Vire, J.-M. Kauffmann, Analyst 125 (2000) 79.
[27] Y. Okawa, M. Nagano, S. Hirota, H. Kobayashi, T. Ohno, T. Watanabe, Biosens. Bioelectron. 14 (1999) 229.
[28] C. Sun, W. Li, Y. Sun, X. Zhang, J. Shen, Electrochim. Acta 44 (1999) 3401.
[29] M. Valcárcel, M.D. Luque de Castro, Flow-Through (Bio) Chemical Sensors, Elsevier, Amsterdam, 1994, p. 369.
[30] J. Kulys, U. Bilitewski, R.D. Schmid, Bioelectrochem. Bioenerg. 26 (1991) 277.
[31] C. Ruan, F. Yang, C. Lei, J. Deng, Anal. Chem. 70 (1998) 1721.
[32] P.N. Bartlett, P.R. Birkin, J.H. Wang, Anal. Chem. 70 (1998) 3685.
[33] M. Valcárcel, M.D. Luque de Castro, Flow-Through (Bio) Chemical Sensors, Elsevier, Amsterdam, 1994.
[34] K. Matsumoto, J.J. Baeza Baeza, H.A. Mottola, Anal. Chem. 65 (1993) 636.
[35] C. Danilowicz, E. Cortón, F. Battaglini, J. Electroanal. Chem. 445 (1998) 89.
[36] J. Hernandez-Ruiz, M.B. Arnao, F. Garcia-Canovas, M. Acosta, Biochem. J. 354 (2001) 107.
[37] A. Asokan, J.S. De Ropp, S.L. Newmyer, P.R. Ortiz de Montellano, G.N. La Mar, J. Am. Chem. Soc. 123 (2001) 4243.
[38] H.K. Baek, H.E. Van Wart, Biochemistry 28 (1989) 5714.
[39] J.N. Rodriguez-Lopez, M.A. Gilabert, J. Tudela, R.N.F. Thorneley, F. Garcia-Canovas, Biochemistry 39 (2000) 13201.
[40] W. Wang, S. Noël, M. Desmadril, J. Guéguen, T. Michon, J. Biochem. 340 (1999) 329.
[41] R. Nakajima, I. Yamazaki, J. Biol. Chem. 255 (1980) 2067.
[42] J.B. Wittenberg, R.W. Noble, B.A. Wittenberg, E. Antonini, M. Brunori, J. Wyman, J. Biol. Chem. 242 (1967) 626.
[43] D. Cai, M. Tien, Biochemistry 29 (1990) 2085.
[44] R.W. Noble, Q.H. Gibson, J. Biol. Chem. 245 (1970) 2409.
[45] M. Valcárcel, M.D. Luque de Castro, Flow Injection Analysis. Principles and Applications, Ellis Horwood, Chichester, UK, 1987, p. 59.
[46] P. Richter, B. López Ruiz, M. Sánchez-Cabezudo, H.A. Mottola, Anal. Chem. 68 (1996) 1701.
[47] J.C. Giddings, Dynamics of Chromatography Part I: Principles and Theory, Dekker, New York, 1975, pp. 217–224.
[48] P.B. Hamilton, D.C. Bogue, R.A. Anderson, Anal. Chem. 32 (1960) 1782.
[49] K. Stulík, V. Pacáková, Electroanalytical Measurements in Flowing Liquids, Ellis Horwood, Chichester, UK, 1987, p. 44.
[50] J. Raba, H.A. Mottola, Anal. Biochem. 220 (1994) 297.
[51] J. Raba, H.A. Mottola, Anal. Chem. 66 (1994) 1485.
[52] V.G. Levich, Physicochemical Hydrodynamics, Prentice-Hall, Englewood Cliffs, NJ, 1962.
[53] J. Marcos, A. Ríos, M. Valcárcel, Anal. Chim. Acta 283 (1993) 429.